NUCLEUS–NUCLEUS POTENTIAL AT NEAR-BARRIER ENERGIES FROM SELFCONSISTENT CALCULATIONS

Janusz Skalski

A. Sołtan Institute for Nuclear Studies
Hoża 69, 00-681, Warsaw, Poland
e-mail: jskalski@fuw.edu.pl

(Received December 12, 2002)

Dedicated to Adam Sobiczewski in honour of his 70th birthday

We determine the static nucleus–nucleus potential from Hartree-Fock (HF) calculations with the Skyrme interaction. To this aim, HF equations are solved on a spatial mesh, with the initial configuration consisting of target and projectile positioned at various relative distances. For a number of reaction partners, the calculated barrier heights reasonably well compare with those extracted from the measured fusion and capture cross sections. At smaller target-projectile distances, our results show the intrinsic barriers to heavy compound nucleus formation. We speculate on their possible connection with the fusion hindrance observed for large $Z_{\rm T}Z_{\rm P}$.

PACS numbers: 25.70.Jj, 21.60.Jz

1. Introduction

The experimental synthesis of the heaviest elements depends on the dynamics of nuclear fusion. Overcoming the fusion barrier is the first stage of this process, followed by the compound nucleus (CN) formation and then its deexcitation. The difficulty in making very heavy systems lies not only in the high fission probability of the newly formed excited CN, but also in the substantial hindrance of the CN formation. This hindrance is observed experimentally as a large probability of quasifission in reactions between targets and projectiles with the large charge product $Z_{\rm T}Z_{\rm P}$ >1800. In spite of many efforts spent on its theoretical modelling, the phenomenon of fusion hindrance is still not sufficiently well understood. In its explanation, the crucial role of dissipation of collective motion is usually invoked, as it was done in [1,2], where the fusion hindrance was expressed in terms of the so

called extra-extra-push energy above the fusion barrier, needed in order to produce CN.

Nucleus–nucleus potential, as encountered in the heavy ion collisions at energies close to the fusion barrier, is important for the understanding of the two first stages of the heavy ion fusion reaction. In this work, we provide its picture on the basis of the selfconsistent Hartree–Fock (HF) theory. Starting from an initial configuration of target and projectile at the specific distance R, we calculate the lowest possible final HF state and its energy. Such treatment involves polarization effects meant in the following sense: Two approaching nuclei adjust their matter and charge densities to their mutual long-range Coulomb and short-range nuclear interaction. This induced correlation reduces somehow the total energy of the two fragments as compared to energy they would have remainig in their ground states. As it turns out, using this method we obtain adiabatic potential at large distances (and thus also adiabatic fusion barrier), but excited configurations for smaller distances, deeper in mononuclear regime.

As it was often argued, a non-adiabatic fusion barrier may be expected in actual heavy ion collisions due to the short time scale involved in passing over the barrier. Nevertheless, we think that the adiabatic potential is a necessary ingredient in a selfconsistent study of nuclear fusion in much the same way as the static barrier is a necessary first step in a study of nuclear fission. Difficulty in reaching the adiabatic HF state when starting from overlapping target and projectile may signal a kind of dynamical fusion hindrance.

We notice, that the mean field study essentially contains the same physics as the alternative coupled channels (and transfer channels) approach. The coupling to collective excitations is replaced by various deformations (or more generally, degrees of freedom) of the mean field. Inaccuracies of both methods are complementary: The lack of good quantum numbers in the mean-field vs. schematic couplings of channels. The coupled channels approach, however, seems impractical for very heavy systems.

Within the mean field, for a deformed target or projectile, there is not one, but many fusion barriers, depending on the relative orientation of the fragment symmetry axes with respect to the relative distance vector. These represent some weighted averages over barriers in various quantum states with definite intrinsic and relative angular momenta. In particular, the configuration with the symmetry axis of the deformed fragment perpendicular (parallel) to the relative distance vector corresponds to the side (tip) collision. Quite recently, experimental evidence was presented [3–5] showing that at least part of the CN formation hindrance is related to the dominance of quasifission in tip collisions.

We have performed HF calculations for a number of target-projectile combinations and found the nucleus–nucleus potential and the (outer) adiabatic fusion barrier. For deformed targets, we have calculated potentials for both tip and side collisions. We have used mostly the Skyrme SkM* interaction [6], originally invented to properly fit the fission barriers. We are aware of one similar HF calculation of the potential energy in a dinuclear system [7], where, however, scission of ^{240}Pu was the main objective.

Since this calculation may be considered as a test of the method as much as a prediction, we include in our study some systems with well measured fusion cross sections in addition to the ^{48}Ca-induced reactions used in recent experiments at JINR in Dubna which, according to the reports [8–10], lead to the synthesis of the heaviest elements. We test our results against experimental fusion (capture) barriers and make comparison to recent calculations within the frozen density regime [11]. We close with some speculations concerning possible relevance of the potentials obtained in our HF study for the fusion hindrance phenomenon.

2. Nucleus–nucleus potential

The potential between nuclei 1 and 2 is calculated as

$$V(R) = E(R) + B_1 + B_2\,, \tag{1}$$

where $E(R)$ is the (negative) HF energy of a dinuclear complex at the distance R and B_i are the (positive) binding energies of target and projectile. In order to have a consistent treatment, B_i, $i = 1, 2$, and $E(R)$ are calculated with the same HF code. We reckon that in this way a large part of the inconsistency between the particular Skyrme model and experimental binding energies cancels out. At kinetic energies close to the Coulomb barrier, the terms involving current in the Skyrme energy functional are small and we neglect them, *i.e.* the treatment is static.

Some care has to be taken about the center of mass (c.m.) correction, which usually is calculated within the HF as the average kinetic energy, $\langle t\rangle = \sum_{\nu-occ}\langle\nu \mid \hat{t} \mid \nu\rangle/A$, with ν labelling single particle states, and subtracted from the total kinetic energy. The c.m. correction present in $B_1 + B_2$ is $\langle t_1\rangle + \langle t_2\rangle$. For two widely separated fragments, the c.m. correction in $E(R)$ equals $-\langle t_{12}\rangle = -(A_1\langle t_1\rangle + A_2\langle t_2\rangle)/(A_1 + A_2)$. Thus, with separation tending to infinity, $V(R)$ tends to $(A_2\langle t_1\rangle + A_1\langle t_2\rangle)/(A_1 + A_2)$ instead of zero. In order to preserve the usual meaning of the Coulomb barrier the subtraction of this asymptotic term is understood in Eq. (1).

It has to be emphasized that this subtraction is incorrect for small target-projectile distances, *i.e.* for compact configurations of the system. Somewhere on the way towards CN configuration, kinetic energy of the relative

motion of the two fragments should transform into potential energy of the combined system. Unfortunately, at present, we do not know how to implement this matching. Therefore we do not continue our calculations down to the CN configuration.

It is precisely at small target-projectile distances where a more exact definition of the configuration of the system becomes necessary in order to make Eq. (1) definite. We choose this configuration in the same way as for the large distances, by taking two nuclei at the prescribed c.m. separation as the starting point of the HF iteration. The final HF states obtained from such a starting configuration always have a constriction dividing the system into two pieces, with mass and charge numbers nearly equal to those of target and projectile. Certainly, although for large distances such configurations are natural when studying fusion barriers, in mononuclear regime at smaller distances there are many other configurations, *e.g.* corresponding to other mass and charge asymmetries, or other necking, which may define lower potential $V(R)$.

In the present calculation pairing is neglected. As far as the fusion barriers are concerned, this omission is not expected to induce any sizable effect.

3. Method of calculations

We have solved HF equations on a spatial mesh of a size proper to the colliding system. Our code assumes two plane symmetries, *i.e.* it allows for the mass asymmetry along one direction. Along the same direction both fragments can acquire dipole and other odd-multipole moments. With this symmetry limitation it is still possible to consider tip and side collisions, with the angle between the symmetry axis of a deformed nucleus and the line connecting the centers of two fragments equal to 0° and 90°. Angles in between are outside the scope of the imposed symmetry.

Initially, two sets of wave functions corresponding to two fragments are placed at a chosen distance being an integer multiple of the mesh spacing (in the range 0.5–0.77 fm). Then the HF proceeds by the imaginary-time evolution. Wave functions are kept orthonormal and this enforces the Pauli principle. For fragments placed close enough, the necessary rearrangement of orbitals occurs already at the beginning of the HF procedure and avoids higher than normal densities. Final wave functions correspond to the local minima of the energy functional to which the initial configuration converged. For smaller distances $R = 7$–10 fm, these minima are mostly excited above the adiabatic configuration at the same R.

The distance R between two fragments is calculated as the distance between c.m. of two half-spaces containing A_1 and A_2 nucleons. It changes

during iteration. This change is usually small for larger distances, but it becomes sizable for more compact configurations for which the final distance is always larger than the initial one. In other words, the convergence towards CN configuration by means of the procedure described above turns out to be difficult.

4. Results and discussion

The contour maps of nuclear density corresponding to the tip and side collision barriers for the ^{238}U+^{48}Ca system are shown in Fig. 1. The distance of $\sim$ 14.3 fm between the mass centers of the two fragments at the tip collision barrier is reduced by about 2 fm to $\sim$ 12.5 fm at the side collision barrier. The individuality of the two fragments is well pronounced at both barrier configurations.

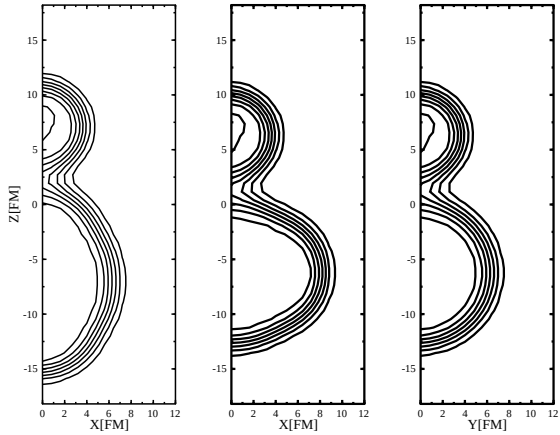

Fig. 1. Density distribution at the fusion barrier for ^{238}U+^{48}Ca system: For tip collision, in plane parallel to the symmetry axis (left), for side collision, in plane parallel to the symmetry axis of ^{238}U (center), and in plane perpendicular to this symmetry axis (right). The planes lie 0.387 fm off the origin, contour lines are drawn every 0.02 fm^{-3}.

The nucleus–nucleus potentials calculated with the SkM* force for six systems are shown in Fig. 2. One can distinguish two types of entrance channel potentials. For smaller $Z_{\rm T}Z_{\rm P}$, after passing the fusion barier, $V(R)$ decreases with decreasing distance. For systems with larger $Z_{\rm T}Z_{\rm P}$, the potential has a minimum behind the barrier, and $V(R)$ rises for smaller distances, sometimes above the barrier. It is quite possible that for R sufficiently small, $V(R)$ rises above the barrier for all heavier systems, although we have not checked it yet. For systems with large $Z_{\rm P}Z_{\rm T} \approx 2500$

(not shown), there is a continuous fall of $V(R)$ with R, *i.e.* there is no minimum, but only a plateau as its remnant. One can observe in Fig. 2, that V rises more steeply with decreasing R for the ^{208}Pb+^{48}Ca system than for reactions with deformed actinides. At $R \approx 8$ fm, $V(R)$ is more than 10 MeV above the fusion barrier in the first case, while it is still under the (side) fusion barrier for the much heavier ^{248}Cm+^{48}Ca system. This would suggest some advantage of the side collisions with prolate deformed targets.

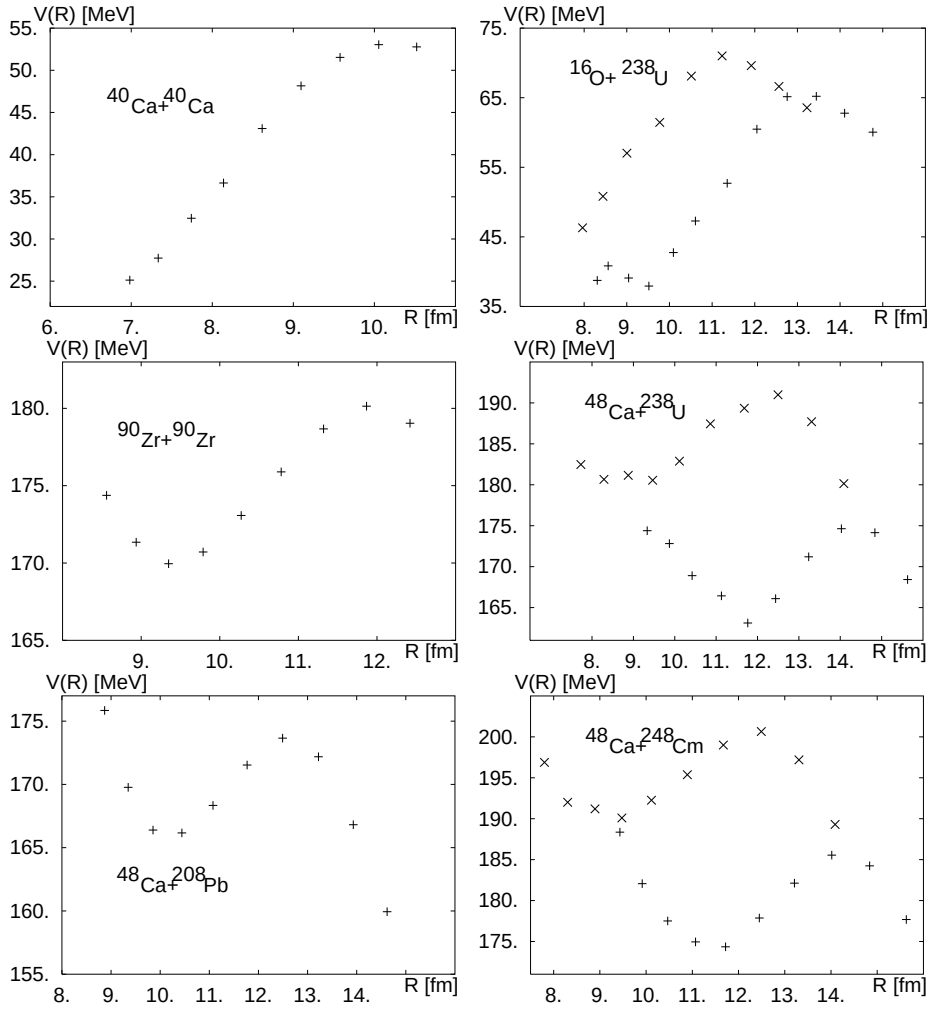

Fig. 2. Nucleus–nucleus potentials obtained with SkM* force, normalized to energy of separated fragments. For deformed targets, both potentials for tip (pluses) and side (crosses) collisions are given.

Comparison of our HF potentials to those in [11], obtained within the frozen density Thomas–Fermi approach, shows that the qualitative features of both potentials are the same. However, there are important quantitative differences: (1) The selfconsistent fusion barriers are systematically lower by 5–10 MeV; (2) The rise of the selfconsistent potentials for smaller distances is much smaller than that seen in [11]. This follows mainly from the fact that, at smaller R, densities in [11] start to double, whereas our densities are always close to normal. This difference is particularly drastic for reactions with actinides, *e.g.* for side collision ^{48}Ca+^{238}U at $R = 7.7$ fm, our $V(R) = 182.5$ MeV, while $V(R) > 230$ MeV in [11]. As a consequence, the minima of $V(R)$, if present, are shifted in [11] towards larger R.

Calculated fusion barriers $B_{\rm cal}$, taken as the locally highest value of $V(R)$, rounded to 0.5 MeV, are compared in Table I to the Bass fusion barriers [12] and to the recently given threshold barriers $B_{\rm thre}$ [13]. The latter quantities are derived from the fusion data and are expected to correspond to the calculated adiabatic barriers. The values of $B_{\rm thre}$ for the heaviest systems are based on the capture data [14]. For deformed targets, both the calculated tip and side (in parentheses) collision barriers are given. Relative to $B_1 + B_2$, the compound nucleus ground states have energies: 14.3 MeV (^{80}Zr), 57.3 MeV (^{130}Nd), 41.1 MeV (^{136}Nd), 157.3 MeV (^{180}Hg), 38.3 MeV (^{254}Fm), 153.8 MeV (^{256}No) [16], and 160.8 MeV (^{286}112), 163.0 MeV (^{292}114), 169.3 MeV (^{296}116), 177.0 (^{298}118) [17].

TABLE I

Calculated fusion barriers for tip (side) collisions in MeV *vs* threshold [13] and Bass fusion barriers [12]. The threshold barrier for ^{90}Zr+^{90}Zr is inferred from [15], that for ^{238}U+^{16}O from [3].

System	$B_{\rm cal}$	$B_{\rm thre}$	$B_{\rm Bass}$
^{40}Ca+^{40}Ca	53	50.2±0.2	53.5
^{90}Zr+^{40}Ca	95	92.7±0.6	102.2
^{96}Zr+^{40}Ca	88.5	87.5±0.3	100.8
^{90}Zr+^{90}Zr	180	∼175.85	195.3
^{208}Pb+^{48}Ca	173.5	169±2	187.4
^{238}U+^{16}O	65 (71)	∼71	85.3
^{238}U+^{48}Ca	174.5 (191)	182±2	206.9
^{244}Pu+^{48}Ca	181 (196.5)	–	210.8
^{248}Cm+^{48}Ca	185.5 (200.5)	–	215.0
^{250}Cf+^{48}Ca	190 (205)	–	219.7

For spherical target and projectile pairs, $B_{\rm cal}$ are slightly larger than $B_{\rm thre}$. The experimental difference in barriers for the reactions of ^{40}Ca on ^{90}Zr and ^{96}Zr is nicely reproduced by our calculations. The calculated barrier for the reaction ^{238}U+^{16}O seems to be lower than that suggested

by the experimental data [3]. For ^{48}Ca+^{238}U, $B_{\rm thre}$ is nearly equal to the average of the calculated tip and side collision barriers. For other heavy actinide targets, there are too few experimental data for extracting $B_{\rm thre}$. However, the data on evaporation residue formation give some idea on the height of the fusion barrier. Two events observed in the reaction on ^{238}U target for $E_{\rm cm}=192.2$ MeV [18], three events for ^{244}Pu target at $E_{\rm cm}=194.5$–202 MeV [19] and one event for ^{248}Cm target at $E_{\rm cm}=199.7$–205.1 MeV [10] suggest similar, or slightly lower, values of the corresponding fusion barriers.

It has to be emphasized that the binding energies B_i of the individual fragments calculated with the SkM* force sometimes differ by few MeV from the experimental values. The hope is that this inaccuracy mostly cancels in $V(R)$ due to subtraction in Eq. (1). This expectation is correct, *e.g.* for the ^{248}Cm+^{48}Ca reaction: Although ^{48}Ca is overbound by the SkM* force by ~ 5 MeV (this nucleus was not included when this force was fitted) and roughly correctly bound by the SkP force [20], the fusion barriers of 185 MeV (200 MeV), calculated with SkP, well agree with the values of Table I.

Although calculated potentials are presented here as functions of the c.m. distance R, one can use conventional multipole moments to characterize deformation of target-projectile systems in a more precise way. For example, for tip collisions of ^{48}Ca on actinides, the distances in Fig. 2 correspond to quadrupole moments varying in the range: $Q = 90 \div 220$ b, octupole deformations $\langle r^3 Y_{30}\rangle = 10 \div 70 \times 10^3$ fm^3, and necking given by the moments $\langle r^4 Y_{40}\rangle = 14 \div 120 \times 10^4$ fm^4. Dipole moments D reach 14–16 efm for the most elongated configurations, while they change sign for more compact configurations. For side collisions, nonaxial moments are present, like $Q_{22} + Q_{2-2}$ and $\langle r^3(Y_{32} + Y_{3-2})\rangle$. For symmetric systems, for which it is easy to define multipole moments of fragments, one finds induced dipole moments D of 0.5-1 efm in ^{40}Ca, and 2–2.5 efm in ^{90}Zr fragments. Induced quadrupole moments Q are small -0.1 b (^{40}Ca) and 0.3 b (^{90}Zr) at most. For asymmetric systems, multipole moments of individual fragments are very sensitive to the way the division of the whole system into two fragments is made.

The most intriguing question coming to mind when looking at Fig. 2 is whether the calculated potentials $V(R)$ have anything to do with the fusion hindrance seen in experiment. They indeed show that the configuration of two approaching fragments leads to the intrinsic barrier for heavy systems. This barrier appears and then becomes more stiff with rising $Z_{\rm T}Z_{\rm P}$. Strictly, this follows from a non-adiabatic character of the potential and may be related to dissipation of collective motion. Phrasing differently, the HF ralaxation of the entrance channel configuration to the adiabatic configuration becomes ineffective at smaller distances R. Further, the barriers for tip and side collisions show that the latter can lead to smaller R, thus favouring CN formation.

On the other hand, the intrinsic barrier appears already for ^{90}Zr+^{90}Zr and ^{208}Pb+^{48}Ca reactions, for which no fusion hindrance is experimentally observed [14,15]. Intuitively, in order to be captured in the CN configuration, a system must pass inside the CN fission barrier, placed at $R_{\rm fis}$. While $R_{\rm fis}$ for the first system (^{180}Hg) is large, so that the intrinsic barrier occurs at $R < R_{\rm fis}$, it is not so for ^{256}No, for which we expect $R_{\rm fis} \approx R_0 = r_0 A^{1/3} \approx 7$ fm. Clearly, some intervening concept of the configuration change when the intrinsic barrier is hit is required in order to explain that the latter reaction leads to CN. Still, such configuration change should incur some probability loss which would lead to some fusion hindrance.

Ultimately, it seems that a more detailed study of competing compact configurations of target and projectile and of configuration changes may lead to a better understanding of the fusion hindrance. We plan to continue our study in this direction.

Enlightening comments of Janusz Wilczyński on the experimental and threshold fusion barriers are gratefully acknowledged.

REFERENCES

[1] W.J. Świątecki, *Phys. Scr.* **24**, 113 (1981).

[2] J. Błocki, H. Feldmaier, W.J. Świątecki, *Nucl. Phys.* **A459**, 145 (1986).

[3] D.J. Hinde *et al.*, *Phys. Rev. Lett.* **74**, 1295 (1995).

[4] S. Mitsuoka *et al.*, *Phys. Rev.* **C62**, 054603 (2000).

[5] K. Nishio *et al.*, *Phys. Rev.* **C62**, 014602 (2000).

[6] J. Bartel *et al.*, *Nucl. Phys.* **A386**, 79 (1982).

[7] J.F. Berger, M. Girod, D. Gogny, *Nucl. Phys.* **A502**, 85c (1989).

[8] Yu.Ts. Oganessian *et al.*, *Nature (London)* **400**, 242 (1999).

[9] Yu.Ts. Oganessian *et al.*, *Yad. Fiz.* **63**, 1769 (2000) [*Phys. At. Nucl.* **63**, 1679 (2000)].

[10] Yu.Ts. Oganessian *et al.*, *Phys. Rev.* **C63**, 011301(R) (2001).

[11] V.Yu. Denisov, W. Nörenberg, to be published in *Eur. Phys. J.* **A**.

[12] R. Bass, *Nucl. Phys.* **A231**, 45 (1974).

[13] K. Siwek-Wilczyńska, J. Wilczyński, *Phys. Rev.* **C64**, 024611 (2001).

[14] M.G. Itkis *et al.*, in *Fusion Dynamics at the Extremes*, ed. Yu.Ts. Oganessian and V.I. Zagrebaev, World Scientific, 2001, p. 93.

[15] J.G. Keller *et al.*, *Nucl. Phys.* **A452**, 173 (1986).

[16] G. Audi, A.H. Wapstra, *Nucl. Phys.* **A595**, 409 (1995).

[17] W.D. Myers, W.J. Swiatecki, LBL-36803 (1994).
[18] Yu.Ts. Oganessian *et al.*, in *Fusion Dynamics at the Extremes*, ed. Yu.Ts. Oganessian and V.I. Zagrebaev, World Scientific, 2001, p. 81.
[19] Yu.Ts. Oganessian *et al.*, in *Fusion Dynamics at the Extremes*, ed. Yu.Ts. Oganessian and V.I. Zagrebaev, World Scientific, 2001, p. 65.
[20] J. Dobaczewski, H. Flocard, J. Treiner, *Nucl. Phys.* **A422**, 103 (1984).